Soil Dynamics and Earthquake Engineering 29 (2009) 469–482

Contents lists available at ScienceDirect

Soil Dynamics and Earthquake Engineering

journal homepage: www.elsevier.com/locate/soildyn

Site characterization by seismic noise in Istanbul, Turkey

Matteo Picozzi [a,*], Angelo Strollo [a,b], Stefano Parolai [a], Eser Durukal [c], Oguz Özel [d], Savas Karabulut [d], Jochen Zschau [a], Mustafa Erdik [c]

[a] Helmholtz Centre Potsdam, GFZ German Research Centre for Geosciences, Telegrafenberg, 14473 Potsdam, Germany
[b] Institute of Geosciences, Universität Potsdam, Germany
[c] Earthquake Engineering Department, Kandilli Observatory and Earthquake Research Institute, Bogaziçi University, 81220 Çengelköy, Istanbul, Turkey
[d] I.U. Engineering Faculty, Geophysical Engineering Department, Turkey

ARTICLE INFO

Article history:
Received 18 October 2007
Received in revised form
2 May 2008
Accepted 6 May 2008

Keywords:
Istanbul
Seismic noise
Array measurements
S-wave velocity
Resonance frequency

ABSTRACT

Single station seismic noise measurements were carried out at 192 sites in the western part of Istanbul, Turkey. This extensive survey allowed the fundamental resonance frequency of the sedimentary cover to be mapped, and identify areas prone to site amplification. The results are in good agreement with the geological distribution of sedimentary units, indicating a progressive decrease of the fundamental resonance frequencies from the northeastern part, where the bedrock outcrops, towards the southwestern side, where a thickness of some hundreds meters for the sedimentary cover is estimated. The particular distribution of fundamental resonance frequencies indicates that local amplification of the ground motion might play a significative role in explaining the anomalous damage distribution after the 17 August 1999 Kocaeli Earthquake.

Furthermore, 2D array measurements of seismic noise were performed in the metropolitan area with the aim of obtaining a preliminary geophysical characterization of the different sedimentary covers. These measurements allow the estimation of the shear-wave velocity profile for some representative areas and the identification of the presence of strong impedance contrast responsible of seismic ground motion amplification. Comparison of a theoretical site response from an estimated S-wave velocity profile with an empirical one based on earthquake recordings strongly encourages the use of the low cost seismic noise techniques for the study of seismic site effects.

1. Introduction

Istanbul is a megacity of 12 million inhabitants, who are exposed to a significant earthquake hazard. Moreover, the considerable rate of urbanization combined with uncontrolled land use makes such hazard even higher [1].

The main factor controlling the earthquake hazard for Istanbul is undoubtedly the proximity of the North Anatolian Fault, which in the Marmara Sea region forms a complex fault system [1]. From an analysis of the available earthquake records performed by Ambraseys and Finkel [2], the city is estimated to be affected by a medium intensity (epicentral intensity of VII-VIII) earthquake with an average return period of 50 years.

During the Izmit and Düzce 1999 earthquakes, this scenario was worsened by the recognition of site amplifications that were observed to locally modify the ground motion inside the metropolitan area. In particular, as shown by several studies [3–6], the Avcilar district in the western part of Istanbul suffered significant damage, largely due to the amplification of the earthquake ground motion. In fact, for this area, an intensity of VII (MSK) was assigned, while in the other districts of the metropolitan area an intensity of VI (MSK) was generally observed [7,8]. The anomalous amplification of the ground motion observed in the western part of the city is considered to be mainly related to the presence of soft sediments overlaying a competent seismic bedrock. In fact, the thickness and the velocity of the sedimentary layers, as well the impedance contrast between the sediments and the underlying bedrock, are the main parameters affecting the frequency band of the seismic motion that may be strongly amplified by the local conditions. Therefore, recent studies [9,10] have focused on estimating possible site effects in the metropolitan area of Istanbul, and in particular in its western part.

A suitable characterization of local site effects can be performed by estimating local S-wave velocity profiles, or by determining the resonance frequency of the soft soil layers. Often, information is obtained through invasive techniques, such as drilling, down/cross-hole measurements, etc. However, due to their expensive nature, the widespread application of such techniques is only able to be performed after coming to a compromise with respect to cost, resulting in a limited

* Corresponding author. Tel.: +49 331 2881285; fax: +49 331 2881204.
E-mail address: picoz@gfz-potsdam.de (M. Picozzi).

0267-7261/$ - see front matter © 2008 Elsevier Ltd. All rights reserved.
doi:10.1016/j.soildyn.2008.05.007

exploration depth. In fact, microzonation works are frequently based on the use of the average shear-wave velocity in the uppermost 30 m (Vs30), which is adopted by the National Earthquake Hazard Reduction Program (NEHRP) classification in the USA. However, several works [11–15] have showed that in a number of geological–geotechnical and morphological contexts, the Vs30 classification is not always a suitable tool for site-effect estimation. Also for this reason, non-invasive and cost effective passive seismic techniques have recently become an attractive option for seismic site-effect studies.

Especially in the last decade, environmental noise recordings performed by single station methods to estimate *horizontal-to-vertical* (*H*/*V*) spectral ratio curves [16,17] and by 2D micro-array techniques to estimate surface wave dispersion curves [18] have provided very promising results.

Parolai et al. [19,20] showed that the seismic noise *H*/*V* curves exhibit a good agreement with the *H*/*V* from earthquake recordings, especially with regard to the value of the fundamental resonance frequency of the sedimentary cover. Therefore, performing a large number of noise measurements over a region of interest allows a map of the fundamental frequencies to be obtained, which provides an overview of the distribution of both the sedimentary cover thickness and, most importantly, of those areas where the amplification of the seismic motion in the frequency band of interest for buildings behaviour is expected.

Concerning 2D arrays, it has been shown [21–23] that by using Rayleigh wave dispersion curves, the characterization of the local S-wave velocity profile can be obtained with a good accuracy, especially when a priori information about the total sedimentary cover thickness is available in advance. Further improvements are obtained by applying the joint inversion of phase velocity and *H*/*V* ratio curves [18,24,25], which allows the trade-off problem between the model parameters that hampers the separate inversion of these curves to be overcome. The application of this inversion scheme has also had success in estimating the S-wave velocity profile for sedimentary covers hundreds of meters thick [24]. Although for the engineering-geotechnical community, the lack of high resolution in the S-wave velocity profile can be considered a drawback, from the site-effect point of view, passive techniques, especially in the case of sedimentary cover thicker than 30–50 m, provide estimates of the local transfer function that are in very good agreement with both the empirical ones [26,27] and those obtained by 1D techniques (e.g., SASW and MASW) that allow the reconstruction of the shallower part of the S-wave velocity profile with a higher resolution [28].

In this work, as a preliminary activity for the microzonation characterization of Istanbul, 192 single station measurements (Fig. 1a) for the estimation of the *H*/*V* curves were carried out in the western part of the metropolitan area, in order to estimate the fundamental resonance frequency of the sedimentary cover. In particular, 42 of these noise measurements were performed at sites where accelerometers belonging to the permanent and temporary networks operated by the Kandilli Observatory and Earthquake Research Institute (KOERI) are located. Thus, for 29 sites of the considered accelerometric stations, the *H*/*V* curves from noise recording were compared with those calculated using weak motion recordings. This comparison of the results provided by the different methods was in fact directed towards performing a calibration of the passive seismic techniques in the area investigated, allowing a preliminary validation for the reconstructed sediment–bedrock interface geometry and the site-effects estimates.

In addition, in order to provide additional useful information for site effects and microzonation studies, a series of eight 2D micro-array measurements utilizing short-period sensors and high dynamic digitizers were carried out in selected sites of the study area. The extended spatial autocorrelation technique (ESAC; [22,29,30]), and frequency–wavenumber analysis (maximum likelihood method; [31,32]) were used for the estimation of the Rayleigh wave dispersion curves and wavefield analysis. For the first time, the resulting dispersion curves were used together with the *H*/*V* curve in a joint inversion scheme for the estimation of the S-wave velocity profiles in a megacity. Finally, theoretical site responses were calculated from the S-wave velocity profiles obtained from the micro-array data using the propagator matrix method for a 1D-layered medium [33].

2. Geological setting

The western part of Istanbul is characterized by two main geological settings; the northern and northeastern sections that are dominated by Paleozoic bedrock, and the southern and western parts that are mainly covered by geologically softer sediments (Fig. 1b) [34]. The Paleozoic basements consist of Devonian limestone formations (Trakya, Dolayoba). The upper Miocene sediments and sedimentary rocks that extend over the Paleozoic bedrock are divided into the following units:

- the Bakirköy formation of the upper Miocene, consisting of alternating white, porous, chalky and medium to hard limestone, marl and clay layers;
- the Güngören formation of the middle Miocene, composed of green coloured fissured clay, highly plastic, thin laminated clays, marl and clayey siltstone;
- the Cukurcesme formation, which contains dense to very dense sand, silty sand, clayey sand, gravel and clay;
- the Late Quaternary Kusdili formation, which consists of clay with molluscs, sand, silt and mud, covering the southern coast of Kucukcekmece Lake and the Golden Horn;
- the Alluvial deposits of Quaternary age, consisting of unconsolidated sediments composed of gravel, sand, silt and clay, which overlay the other formations and are the result of fluvial activity; and
- anthropic construction material, overlain by a layer of gravel of a few decimeters, and filled with about half a meter of soil. All of these materials overlie the alluvium and the other formations in some part of the city, reaching a total thickness of approximately 2 m.

Alluvial deposits and other sediments and softer sedimentary rocks represent the most important geological units from the point of view of site effects. In fact, due to the contrast between their generally poor mechanical characteristics and those of the Paleozoic bedrock, strong site amplification of the ground shaking can be expected.

3. Single station measurements

3.1. H/V spectral ratio data analysis

From 24 June to 15 July 2007, an extensive survey of single station seismic noise recordings was carried out over the western metropolitan part of Istanbul. In total, 192 sites were investigated, 42 of which were performed at the accelerometric sites of the Istanbul Earthquake Rapid Response System (IERRS) operated by the Kandilli Observatory and Earthquake Research Institute of Bogazici University, and eight carried out using data collected at 2D array sites (see Section 4). Seismic noise measurements were carried out using seismic stations equipped with the EDL 24-bit digitizer connected to a Mark L-4C-3D 1 Hz sensor with GPS

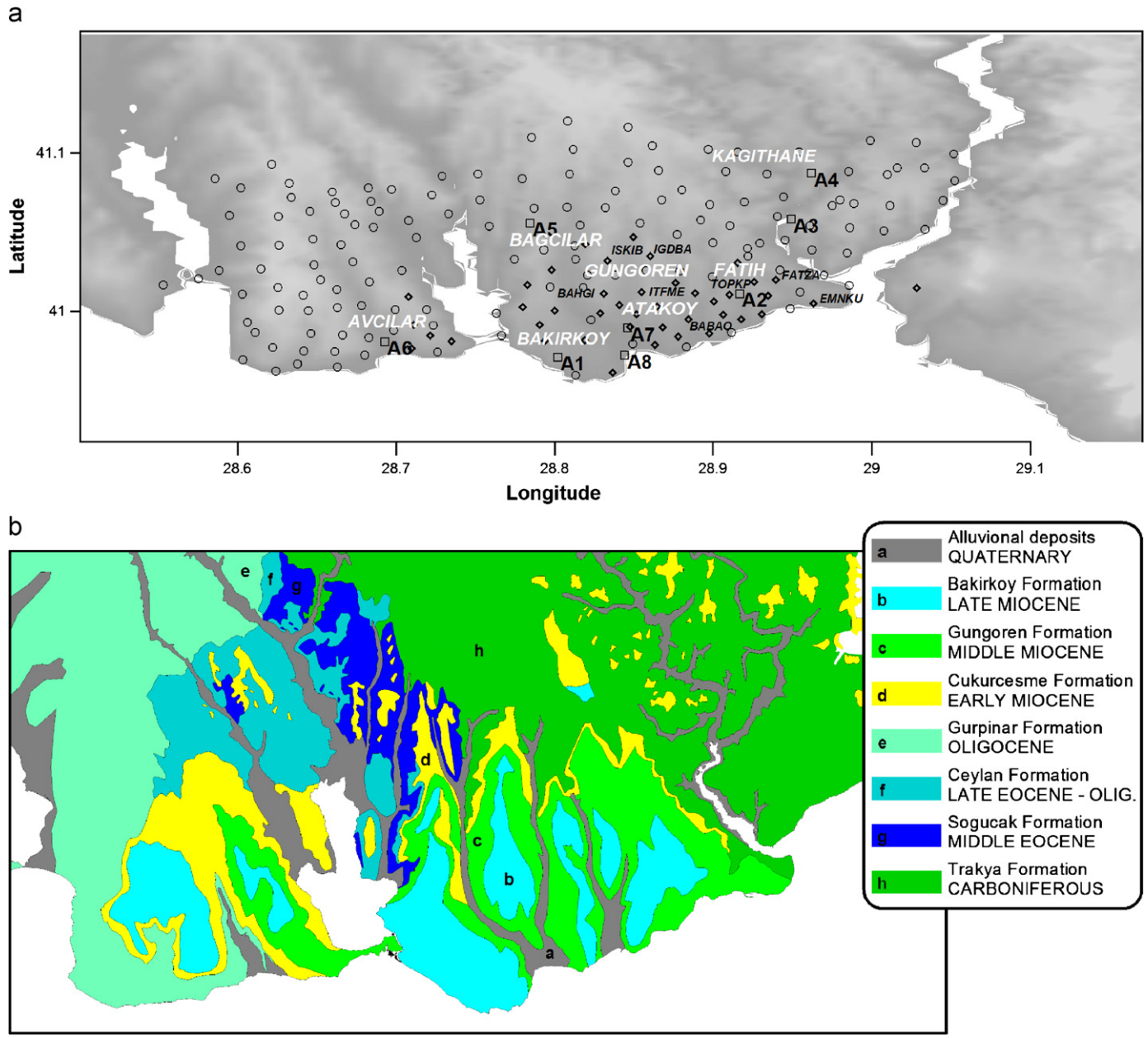

Fig. 1. Western part of Istanbul: (a) single station noise measurements at free field sites (dots), IERRS stations (rhombus, name of stations with earthquake recordings is indicated), and 2D array measurements (squares); (b) geological map.

timing. All the sensors were calibrated, and, as showed by Parolai et al. [19], can be used to reliably analyze frequencies lower than 1 Hz. Following Strollo et al. [35,36], the maximum possible gain for the digitizer (i.e., 10) was used in order to reduce instrumentation self-noise effects. This allows the estimation, also in the case of the most unfavorable scenario where seismic noise approaches the minimum new low-noise model (NLNM) of Peterson [37], of unbiased fundamental frequencies down to at least about 0.2 Hz. Sensors were installed so as to obtain a good coupling between the instrument and soil, and where possible, avoiding asphalt. Moreover, sensors were covered in order to reduce any interference caused by wind. Ambient seismic noise was recorded at 100 Hz sampling rate for about 20 min, which guarantees the statistical stabilization of the signal [38].

The H/V spectral ratios [39] were computed using 20 non-overlapping time-windows of noise recording signal, each window 60 s long and tapered with a 5% cosine function before the computation of the spectra. The Fourier spectra were computed for each noise component and smoothed using a Hanning window of 10% relative bandwidth. This ensures the reduction of numerical instabilities while preserving the major features of the spectra, especially the flanks of the H/V ratios maxima. The resulting spectral ordinates relative to horizontal components were geometrically averaged and divided by the vertical spectral ordinate to compute the H/V function. Moreover, the time stability of the spectral ratios over the recording length was verified in order to avoid the presence of spurious H/V peaks. Whenever H/V ratios determined by transient signals were observed, the relevant portions of recordings were rejected. Although this procedure does not bias the average H/V, it reduces the variability of the confidence interval [40]. Finally, H/V ratios obtained by considering the resultant time-windows (i.e., between 10 and 20) were then averaged to compute the final H/V curve along with the relevant 95% confidence interval (Fig. 2).

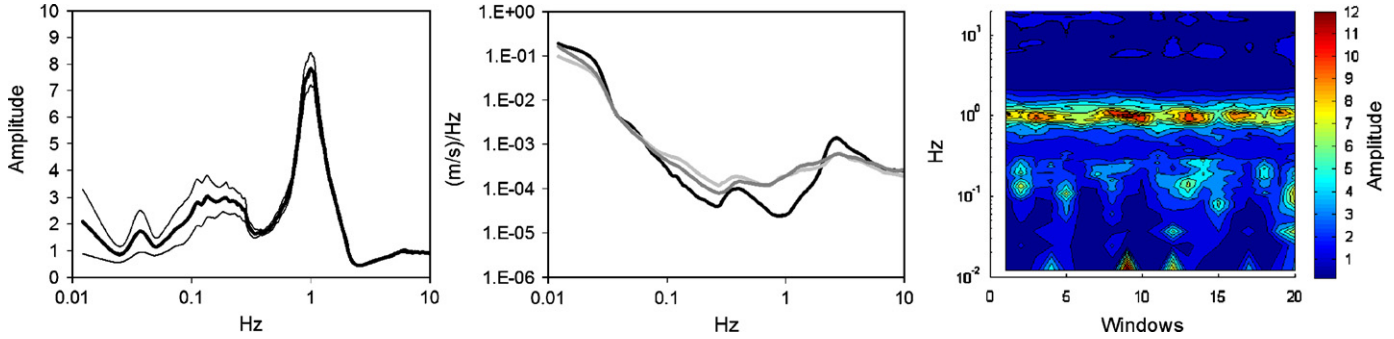

Fig. 2. (Left) *H*/*V* spectral ratio curve ±95% confidence interval; (middle) ground motion amplitude spectra for the vertical component (black), the north–south component (dark grey), and the east–west component (light grey); (right) contour plot of the *H*/*V* spectral ratio time stability.

Table 1
Location, magnitude and source parameters of the earthquakes discussed in this work

Event	Latitude	Longitude	Depth (km)	Mw/ML	Moment (dyne cm)
16 May 2004	40.868	29.268	16.7	4.2/4.3	2.07E22
29 September 2004	40.780	29.020	12.4	4.1/4.0	1.73E22

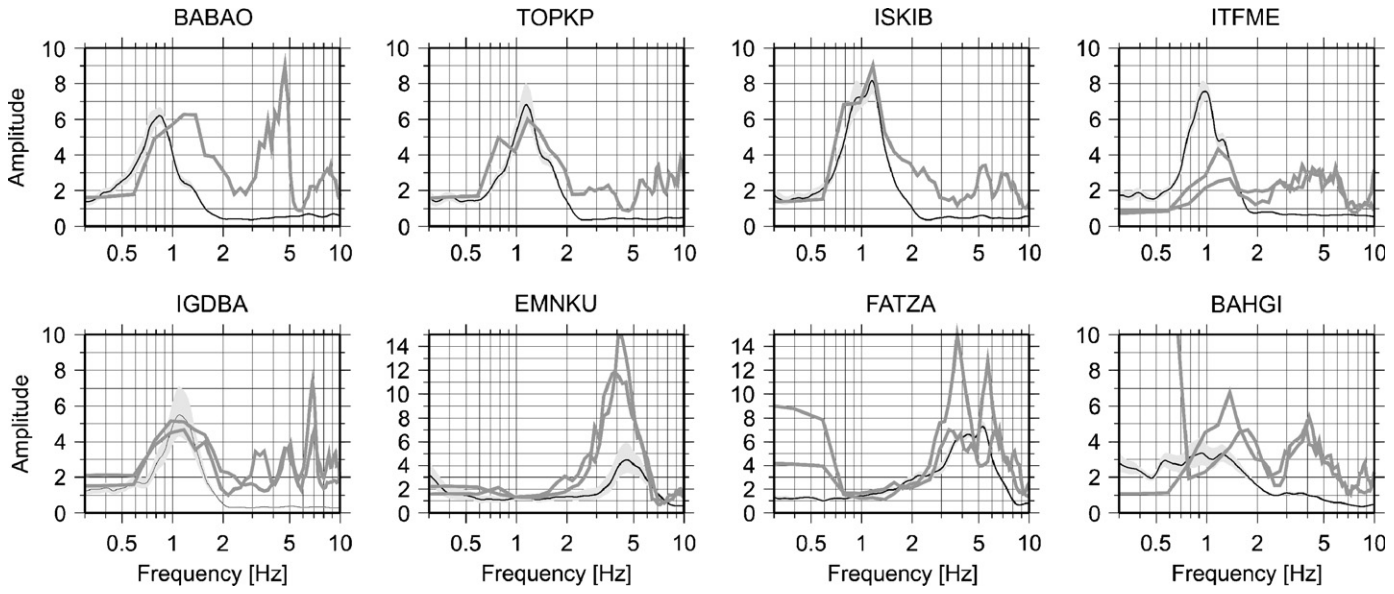

Fig. 3. Average *H*/*V* spectral ratios of noise (black line) ±95% confidence interval (grey area) and *H*/*V* spectral ratios (dark grey lines) of one earthquake with *M*~4 recorded by IERRS stations BABAO, TOPKP and ISKIB, and two earthquakes with *M*~4 by IERRS stations ITFME, IGDBA, EMNKU, FATZA and BAHGI.

3.2. *H/V analysis of small earthquake recordings*

Recordings of two local earthquake events with magnitude ML of 4.1 and 4.2 (Table 1) were available for 29 accelerometric station sites of the IERRS [41]. The Fourier spectra of the events were computed using zero-baseline corrected and cosine tapered acceleration recordings of the three components. Therefore, 5 s time-windows starting 0.5 s before the S-onset [34] were selected. The spectral amplitudes from the two horizontal components were then combined by finding their root-mean-square average. Finally, the *H*/*V* spectral ratio of the earthquake data (*EHV*) were computed.

Fig. 3 compares for some representative sites, the *H*/*V* spectral ratios estimated from seismic noise recordings (*NHV*) from seismic stations and following the procedure previously described, and those obtained using the two earthquake recordings. It is worth noting that, although the number of available earthquake records is limited, the two data sets show a general agreement in the estimation of the fundamental resonance frequencies, f_0, including in some cases their amplitudes as well. Therefore, it is reasonable to have confidence in the reliability of the f_0 estimated by the *NHV* curves.

3.3. *H/V analysis to map soft soil fundamental frequencies*

The single station seismic noise measurement dataset was used with the aim of assessing the fundamental resonance frequency f_0 of soft sedimentary cover. Moreover, the lateral variability in f_0 also allows lateral variations in sedimentary thickness and its dynamic properties to be inferred.

Only in one case was the *H*/*V* ratio curve severely affected by low frequency disturbance, most likely due to bad soil–sensor coupling and wind. Therefore, a map of f_0 using information from 191 measurement sites was obtained. It is also noted in the

western part of the investigated area that for a large number of measurement sites, multiple peaks in the H/V curves were observed, in particular, those sites that typically show a first maximum in the frequency range between 0.15 and 0.3 Hz, and a second one at frequencies higher than 0.5 Hz (Fig. 2). The presence of multiple peaks is interpreted as indicating the presence of multiple impedance contrasts at different depths. In this paper, while drawing the map of resonance frequencies we considered the higher frequencies (i.e., with H/V maxima in the frequency range from 0.5 to 10 Hz) to be related to a shallower impedance contrast than those at very low frequencies (Fig. 4a). In fact, the shallower impedance contrasts probably determine the amplification in a frequency band closer to the fundamental resonance frequencies of buildings, and would be a better indicator of the local increase in damages.

Considering the effect of instrumental self-noise in biasing the H/V shape, as showed by Strollo et al. [35,36], the resulting fundamental resonance frequencies were considered reliable at least until 0.2 Hz, since in the favourable condition of a level of seismic noise higher than the NLNM, the instrumentation used allows the estimation of reliable H/V values down to nearly 0.15 Hz.

Analysing the resulting map of resonance frequencies (Fig. 4a), it is straightforward to identify some general characteristics of the investigated area:

- the isoline of f_0 equal to 10 Hz indicates that the area with very thin sedimentary cover or outcropping bedrock is mainly on the eastern and northern part of the city;
- the central-southern area (e.g., Ataköy, Bakirköy, Güngören, etc.) is characterized by f_0 decreasing in a northeast–southwest direction from 10 Hz to about 0.3 Hz;
- the westernmost area shows more irregular f_0 features. In fact, in Avcilar, the f_0 are well above 0.5 Hz whereas most are about 1 Hz, while in the north, f_0 decrease until least 0.2 Hz, then increases again.

A comparison between the distribution of f_0 and the geological map (Figs. 4a and 1b) clearly highlights the agreement between the fundamental frequencies and geology. In particular, the f_0 limit

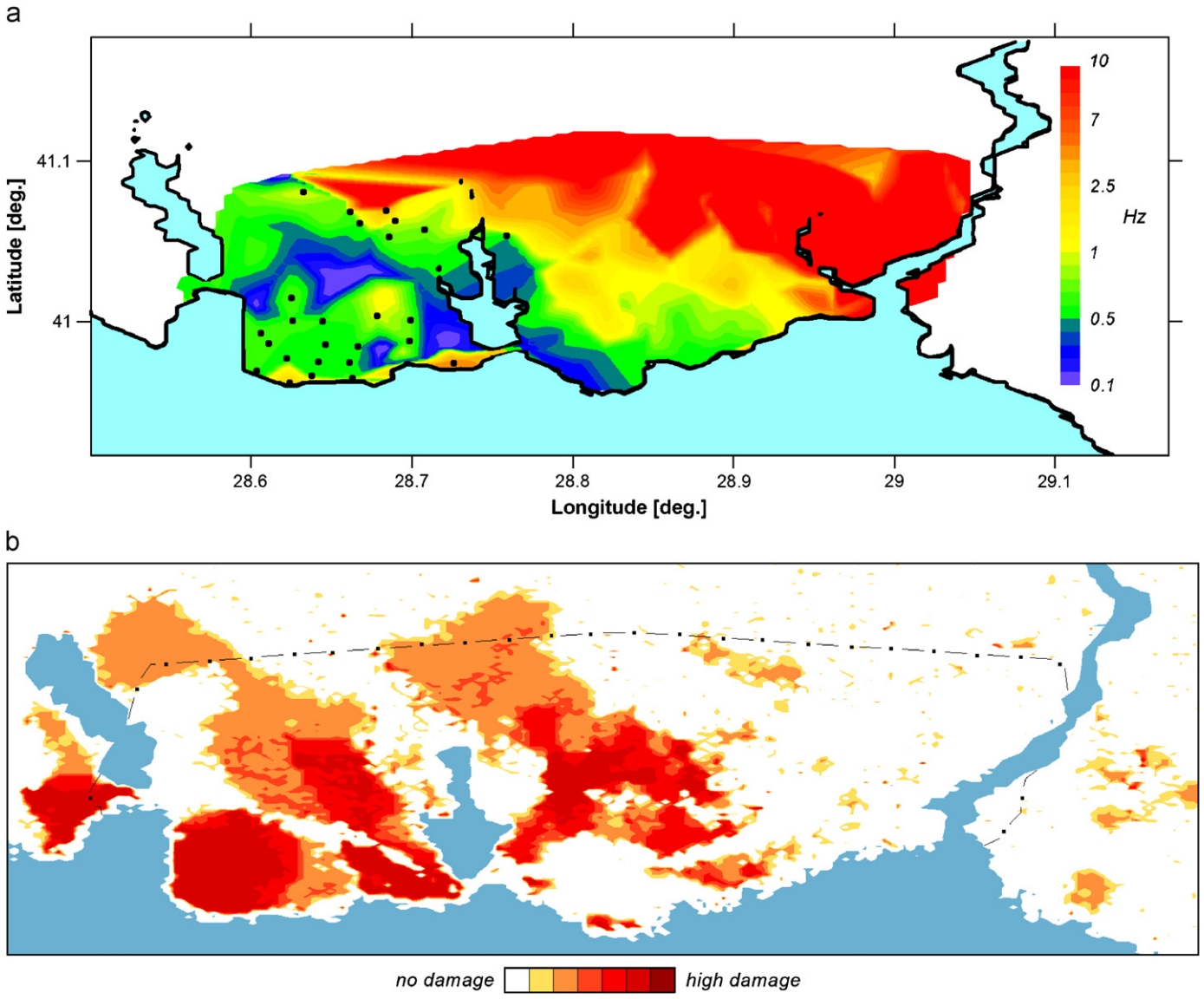

Fig. 4. (a) Map of the resonance frequency of the soil cover in the study area estimated by seismic noise recordings. Measurements where multiple peaks are observed (black dots) are also indicated; (b) distribution of damage in Istanbul 17 August 1999 Kocaeli Earthquake (*redrawn after Istanbul Governorate Disaster Management Centre*). The dotted broken line bounds the investigated area.

of 10 Hz reproduces well the outcropping area of the Trakya and Dolayoba limestone formations. Other significant geostructural characteristics indicated by the f_0 map are as follows:

- for the central part of the investigated area, the very low f_0 (<0.5 Hz) in the Ataköy and Bakirköy districts (Fig. 4a) appears related to the presence of thicker segments of the Bakirköy formation;
- for the western part of the urban area (Avcilar district) f_0 values around 1 Hz are observed, that could be related to the impedance contrast due to the contact between the soft Güngören and Cukurcesme formations overlying the stiff Bakirköy formation.

Several studies [42] have shown that the amplification factor estimated from seismic noise H/V curves is not a reliable proxy for estimating the experimental amplification of a site, since often the seismic noise H/V fundamental frequency amplitude is lower than that estimated from earthquake recordings. Moreover, Picozzi and Albarello [38] showed for a well-constrained test site that, while higher harmonics in the experimental and theoretical site-response function can have higher amplitudes than the fundamental resonance frequency, this information is always missing in the seismic noise H/V curves. For these reasons, the lack of detailed statistically significant comparisons between seismic noise and S-wave site-response amplification, mean that the fundamental resonance amplifications are not taken into account.

Fig. 4b shows the distribution of damage after the 17 August 1999 Kocaeli Earthquake (*after Istanbul Governorate Disaster Management Centre*). As observed in several previous studies [3,9,10,43,44], the role of site effects in the damage distribution in the western part of Istanbul was considerable for this event. Although a discussion of the observed damage after the 17 August 1999 Kocaeli Earthquake is beyond the scope of this microzonation study, since information about the vulnerability of the structures in question is not available, we will consider a qualitative comparison between the f_0 map and the distribution of damage. In particular, the boundary between the "no damage" and "consistent damage" areas in the eastern and northern parts of the study area corresponds quite well to the isoline for the 10 Hz f_0 map. Thus, at a first glance it is clear that the most damaged areas are located in the part of the city mainly covered by geologically softer sediments, where f_0 spans the frequencies of interest for buildings (i.e., from 0.5 to 10 Hz). Local differences may, of course, be due to vulnerability variations. Therefore, we believe that the f_0 map provides a valuable tool for identifying areas of a city that could experience heavier damage from future earthquakes due to the unfavorable geological conditions.

4. Array measurements

The S-wave velocity profiles were experimentally derived from seismic noise recordings carried out using arrays of sensors [30]. Considering the high geological heterogeneity characterizing the investigated area, sensor arrays were installed at sites with different surficial geology (Fig. 1 and Table 2). The 2D array geometries were slightly variable due to practical restrictions. The inter-station distance chosen ranged between a minimum of 5 and 10 m, and a maximum between 100 and 150 m, depending on the site. These ranges allow the analysis of a range of wavelengths that guarantee large depths to be investigated, but with still sufficient (i.e., from 5 to 10 m) shallow resolution [30]. A good azimuthal and inter-station distance coverage was guaranteed by the applied geometry (Fig. 5a inner inset).

Table 2
Location of the 2D array

Code	Name	Latitude (GPS position)	Longitude (GPS position)
A1	Saruzian Sokak	40°58′15.00″N	28°48′07.00″E
A2	Fatih	41°00′00.00″N	28°55′00.00″E
A3	Miniaturk	41°03′29.00″N	28°56′57.00″E
A4	Kagithane	41°05′14.00″N	28°57′43.00″E
A5	Bagcilar	41°03′20.00″N	28°47′04.00″E
A6	Refinery Esenyurt	40°58′50.00″N	28°41′34.00″E
A7	Ataköy	40°59′21.00″N	28°50′46.00″E
A8	Military Base Bakirköy	40°58′19.48″N	28°50′39.05″E

The GPS position is for the central sensor of the array.

The arrays located in the Ataköy district (A7) and in the "Military area" (A8) consisted of 12 stations equipped with a 24-bit digitizer RefTek connected to a Mark L-4C-3D 1 Hz sensor with GPS timing. The stations recorded for more than 1 h at 100 Hz sampling rate. For A7, due to instrumental malfunctions, data from two stations could not be used.

All other arrays consisted of 13 stations equipped with the EDL 24-bit digitizer and the same sensors of the previous array. Ambient seismic noise was recorded at 200 Hz sampling rate and the stations were operated continuously for about 2 h.

Before the analysis, all recordings were corrected for the instrumental response, considering the calibration parameters of each sensor. The H/V curves were computed for all stations of each array, following the procedure described previously.

4.1. Phase velocity analysis

For estimating dispersion curves of Rayleigh waves, a total of 120 non-overlapping signal windows of vertical component recording, each window being 30 s long, where considered.

In this study, the Extended Spatial AutoCorrelation (ESAC; [22,29,30]) and the frequency–wavenumber (FK), specifically the maximum likelihood method (MLM; [31,32]), methods were adopted.

Computing the Rayleigh wave dispersion curve by the ESAC procedure [22], we followed both the procedure described by Parolai et al. [23], and a different approach that allowed us to estimate the statistical uncertainties for the average phase velocity. Accordingly, the spatial correlation coefficients estimated for each singular time-window were fitted with Bessel functions. In this way, for each frequency, the average phase velocity is obtained from the resultant 120 velocity samples. As shown in Fig. 5a, the two approaches provide equivalent average estimates, but the redundancy of information of the second approach allows the 95% confidence interval for the average phase velocity to be evaluated.

The MLM–FK analysis [31,32] is performed by a coherence matrix evaluation, which is used for computing the FK power spectral density function (PSDF). The location of a peak in the PSDF provides information about both the apparent propagation velocity and the azimuth of the signal recognized from the array. It has been shown [28,30] that FK techniques show a tendency to overestimate the phase velocity with decreasing frequency with respect to ESAC. However, the FK estimates, differently from ESAC, allow the direction from which the main sources of energy originate to be resolved. This is especially important in urban area, where the sources of microtremors may not be randomly distributed, and therefore the basic assumption of the ESAC method not verified. Moreover, MLM–FK may help to discriminate between the contributions of higher modes of surface waves to the wavefield.

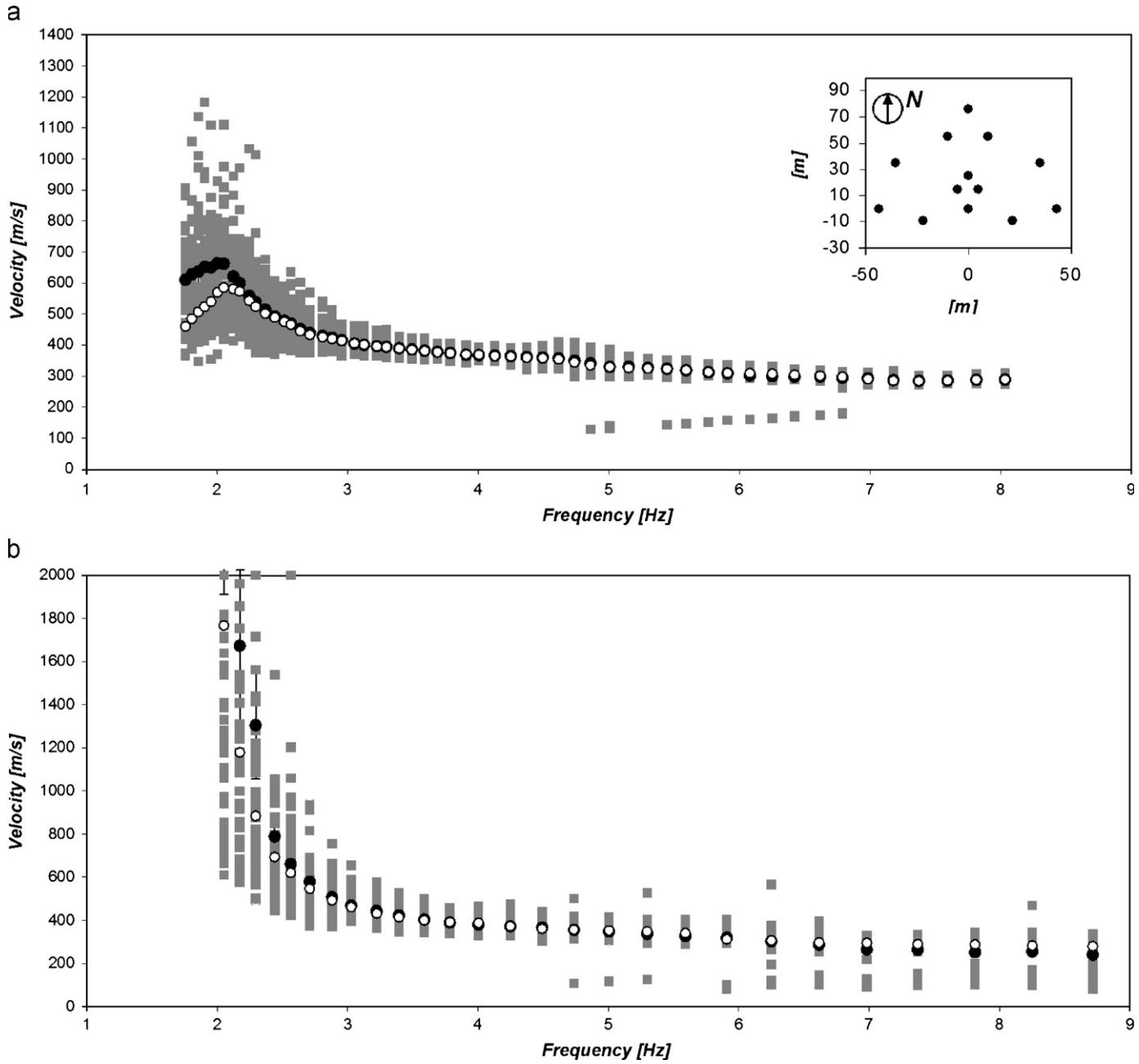

Fig. 5. (a) ESAC dispersion curve for seismic noise recordings of array A2 using singular time-windows analysis (grey dots) and average values (black dots), and from the classical approach following Ohori et al. [22] (white dots). (Inner inset) Array configuration for A2. (b) Singular time-windows analysis for the same data set similar to (a) but for MLM analysis (grey and black dots), and from the classical approach following Capon [31] (white dots).

The array response and PSDF contour plots of different frequencies were computed for all the arrays. The comparison of these plots allows us to identify secondary peaks due to spatial aliasing (e.g., see 10 Hz in Fig. 6), and to verify the microtremor source distribution (Fig. 6). In most of the analyzed array recordings, the maximum frequency that could be analyzed was around 10 Hz. Also for the MLM method, the velocity analysis was performed by following both the classical strategy, where the averaged PSDF is analyzed (e.g., as proposed by Horike [32]), and by estimating the PSDF of each singular time-window [45]. The two approaches provided nearly equivalent results (Fig. 5b), with the second preferred as it allows a statistical uncertainty to be evaluated. Fig. 7 shows Rayleigh wave dispersion curves derived by array measurements. In general, the variable trends of the dispersion curve reasonably reflect the variable geological conditions existing at the different sites (Fig. 1). In particular, A1, A2, A5, A6 and A7 were installed on surficial deposits where the phase velocity increases almost regularly with decreasing frequency between 2 and 10 Hz. On the other hand, the dispersion curve at A4, which was located on outcropping bedrock, shows a Rayleigh wave velocity of about 2000 m/s, while a low Rayleigh wave velocity (100–200 m/s) and a steep increase at lower frequencies were estimated at the A3 and A8 arrays, indicating that close to the coast, very soft sediments overlie stiff bedrock.

In the cases (e.g., arrays A2, A3, A6 and A7) where the basic assumption of a uniform distribution in space of the stationary and stochastic seismic noise sources is verified, and the wavefield is dominated by the Rayleigh wave fundamental mode, as indicated by the frequency wavenumber PSDF (not shown), the ESAC and MLM curves are in good agreement (Fig. 7). However, in

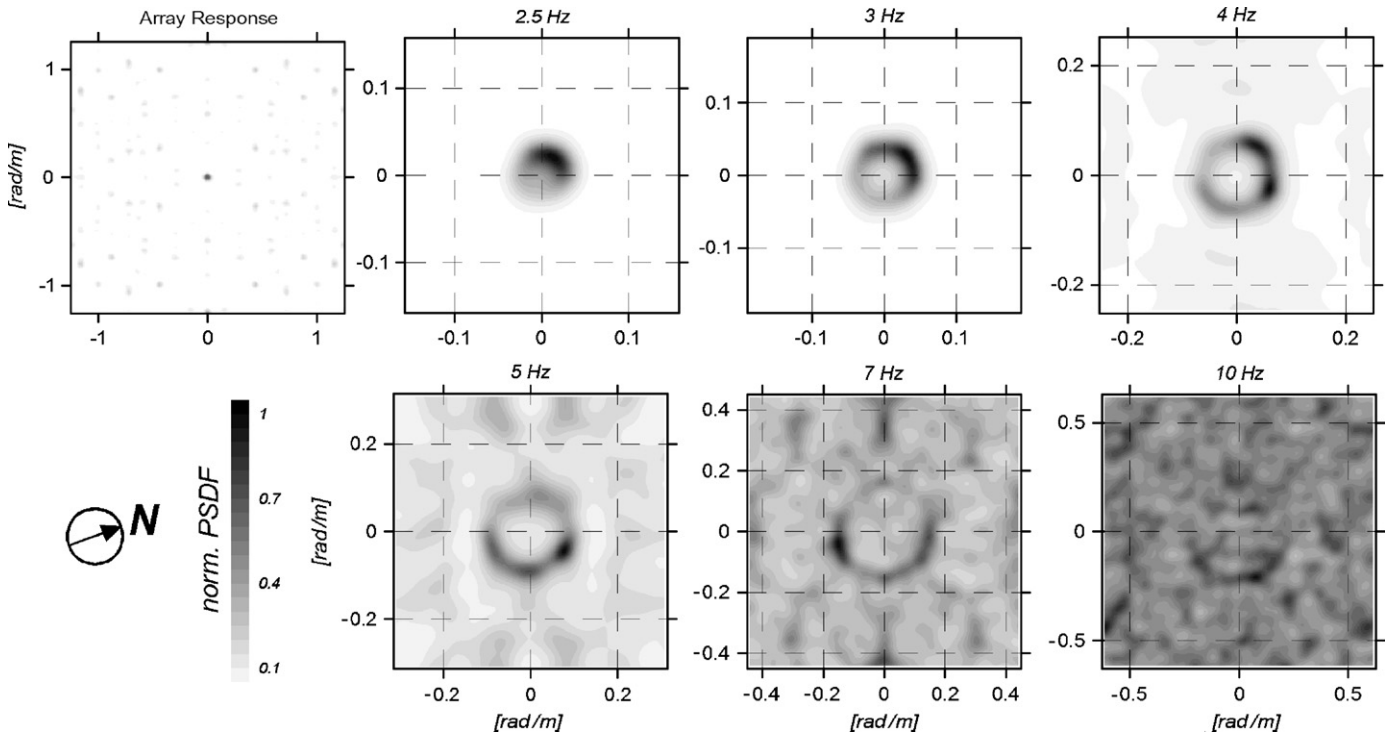

Fig. 6. Results from applying the MLM to the seismic noise recordings of array A2. Array response and contour plots showing for some representative frequency the normalized frequency–wavenumber power spectral density function. The symbol indicates the north direction.

the low frequency range, the MLM curves exhibit, as usual, larger velocities than ESAC. For arrays A1 and A5, at frequencies higher than about 4 Hz, MLM provides phase velocities considerably higher than those from ESAC, that are characterized by a larger uncertainty. This suggests that the wavefield is not dominated by surface waves and the MLM estimation is very sensitive to local spurious maxima in the single record PSDF. In contrast, the ESAC method, with the procedure of fitting the spatial correlation coefficients with a zero-order Bessel function, seems to be more robust in extracting the contribution of dispersive waves. A more detailed investigation of this evidence is well beyond the scope of this paper, but will certainly be taken into account in future methodological studies.

Finally, for arrays A4 and A8, only the MLM method provides coherent dispersion curve results, probably because the basic assumptions of the temporal and spatial noise sources being stationary for the application of the ESAC method were not verified.

4.2. Inversion

For the sites where both high-quality Rayleigh wave dispersion and H/V ratio curves were derived, a joint inversion scheme [24] was used to estimate the local S-wave velocity profile. In particular, the joint inversions of dispersion and H/V curves were performed following the scheme proposed by Picozzi and Albarello [26]. This scheme uses a combination of genetic algorithms and generalized least-squares methods to obtain the global minimum of the non-linear solution fitness. In fact, the genetic algorithm allows a non-linear inversion analysis to be performed that does not depend upon an explicit starting model and allows the identification of the parameter's search space where the global minimum of the inversion problem lies. However, it may only provide a solution close to the global minimum and in some cases be unable to reproduce the experimental data satisfactorily. Therefore, the minimum misfit model from the genetic algorithm inversion can be used as the starting point for the linearized inversion carried out with the generalized least-squares algorithm. Here, the genetic and the generalized least-squares algorithm, respectively, proposed by Yamanaka and Ishida [46] and Arai and Tokimatsu [25], were used. The forward modelling of Rayleigh wave phase velocities and H/V curves was performed using the modified Thomson–Haskell method proposed by Hermann [47] and following the suggestions of Tokimatsu et al. [21] and Arai and Tokimatsu [17], under the assumption of vertically heterogeneous 1D earth models. The validity of this assumption is investigated by computing the H/V curve for each station of the array. Whenever the H/V curves provide the same estimate of the fundamental frequency and the main peak exhibits a good level of shape similarity, it is reasonable to assume that the geological structure underneath the array does not change significantly. Thus, in these cases, the resulting average H/V curve can be safely considered as being representative for the volume underneath the array.

The modelling of both the dispersion and H/V ratio curves during the inversions was not restricted to the fundamental mode only, but included higher modes. During the inversion, the two data sets are weighted in a balanced way by the cost function used by Herrmann et al. [48]. Nevertheless, when the two data sets differ considerably in quality, their relative influence is controlled by a weighting parameter. Obviously, when one of the two experimental curves cannot be used (e.g., because of the presence of industrial noise signals) the proposed inversion scheme can still be applied using only one of either the dispersion or H/V curves.

4.2.1. Results of the inversion analysis and discussion

The results of the inversion analysis for all array measurements are shown in Figs. 8 and 9. For most of the arrays (i.e., A1, A2, A5, A6, A7 and A8), it was possible to perform a joint inversion analysis using dispersion and H/V curves of equivalent quality. Only for arrays A3 and A4 were the inversions performed using the dispersion curve alone. In fact, for A3, the H/V curves at

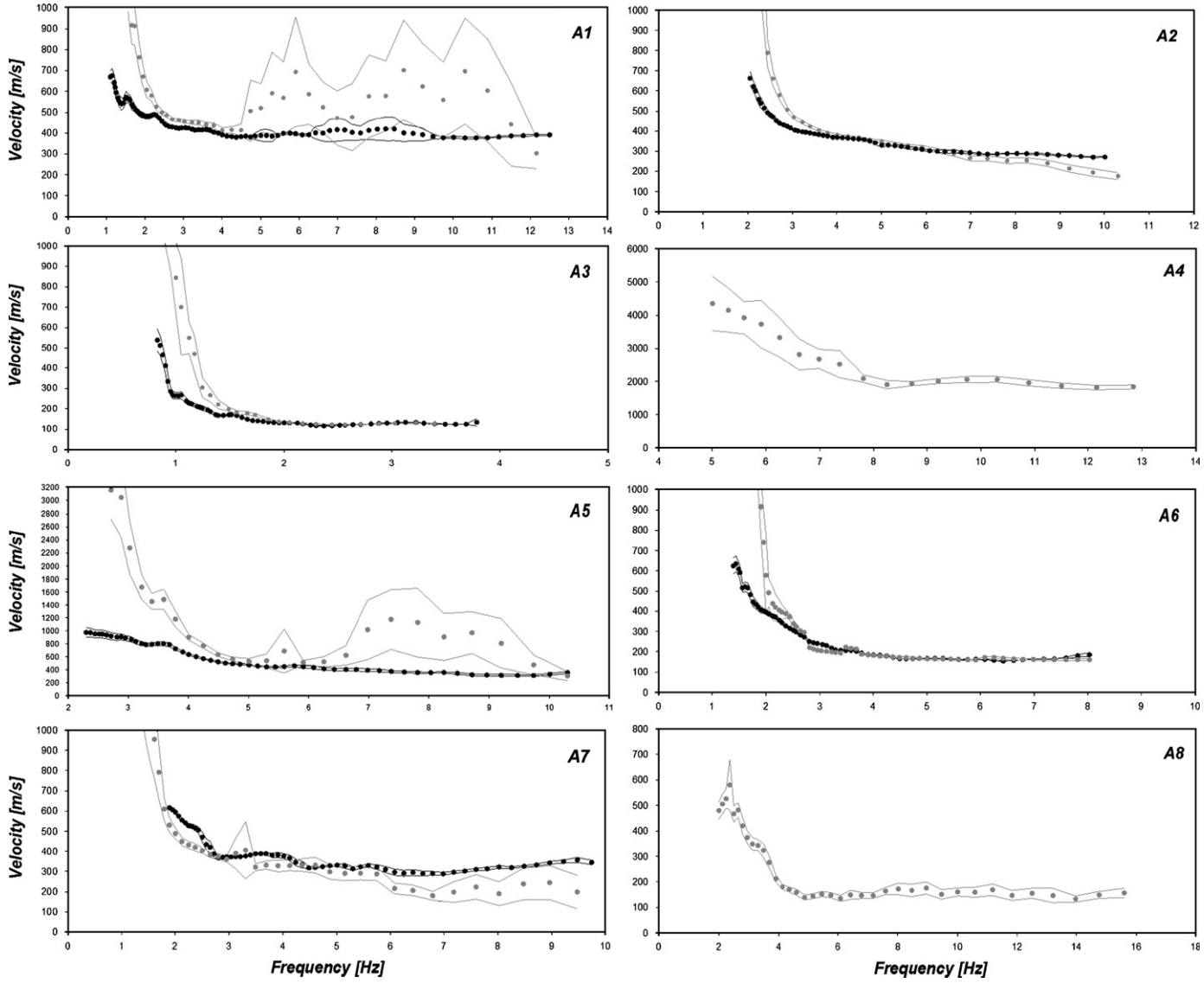

Fig. 7. ESAC (black dots) and MLM (grey dots) Rayleigh wave dispersion curves and relative ±95% confidence interval (thin lines).

different sensors were perturbed close to the f_0 by the presence of spurious, probably industrial, signals, while A4 was executed in the northern part of the city where the Paleozoic bedrock outcrops and, thus, the H/V curve is flat (Fig. 8).

Both the theoretical dispersion and H/V curves fit the observed values well. The reliability of the inversion results is influenced not only by the quality of the input data, but also from the frequency range spanned by the H/V and dispersion curves. For A2, the two experimental curves are partially superimposed in frequency and, therefore, both the final best-fit S-wave velocities and the impedance contrast at about 100 m of depth (in the range of wavelengths covered by dispersion and H/V values) are very well constrained. Similar considerations also hold for A5, which exhibits two high impedance contrasts at about 50 and 250 m. On the other hand, for A1, A6, A7 and A8, the dispersion and H/V curves occupy different frequency ranges (i.e., the fundamental resonance frequency is well below the frequencies of the dispersion curve). In these cases, they carry information for different depth ranges, with the dispersion curve being what mainly constrains the velocity in the surficial part of the model, and the H/V curve providing information about the S-wave velocity and impedance contrasts in the deeper part. However, being constrained by only the H/V curve, this part suffers more from trade-off between parameters [18], with the deeper part of the model being characterized by a higher uncertainty. This is also confirmed by the larger instability of the S-wave velocity profiles having misfits equal to best-fit +10%.

The estimated S-wave velocity profiles provide a valuable overview of the different velocity structures in the western part of Istanbul (Figs. 8 and 9). The large variability and complexity of the velocity structure, characterized by different impedance contrasts, has been previously confirmed by different authors [3,10], and could be responsible for the significant variability in ground motion that lead to the irregular distribution of damage after the 17 August 1999 Kocaeli Earthquake (Fig. 3b). However, with the exception of the very simple situation where soft sediment deposits overlying a hard bedrock, the identification of possible ground motion amplifications simply from the visual inspection of S-wave velocity profiles is not possible, nor advisable. For this reason, considerations concerning the occurrence and magnitude of site effects at the investigated sites are discussed below, where the theoretical site responses are estimated.

Array A4 provides an estimate of about 2000 m/s for the stiff Paleozoic bedrock. Arrays A1, A5, A6, A7 and A8 show similar

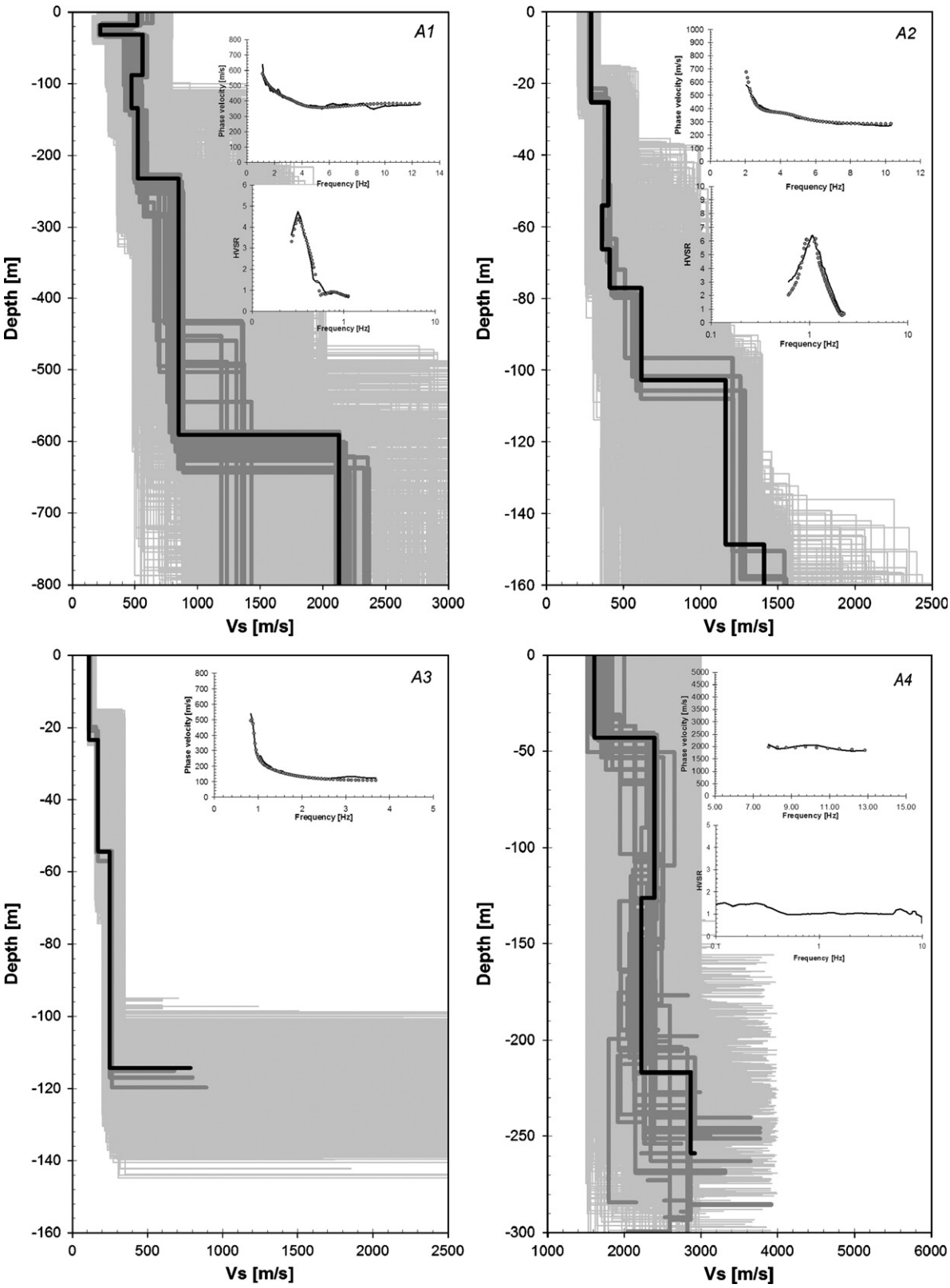

Fig. 8. Inversion results and fit to the dispersion and H/V ratio curves (insets) for the arrays A1, A2, A3 and A4. All four figures show tested models (thin grey lines), the minimum cost model (black line), and models lying inside the minimum cost +10% range (thick dark grey lines). Top inset: observed phase velocities (black line) and the phase velocities for the minimum cost model (grey dots). Bottom inset: average observed H/V ratio (black line) and the H/V ratio for the minimum cost model (grey dots).

high S-wave velocities (around 2000 m/s) at depths greater than 200 m, in agreement with the geology [49], but also suggest complicated layering with high impedance contrasts at shallower depths. For example, both the S-wave velocity profile for A7 in the Ataköy district and that of A8 in the Avcilar area are characterized by a considerable impedance contrast at a depth of about 100 m. In particular, at A7, the S-wave velocity increases from about 600 m/s to about 1000 m/s. These

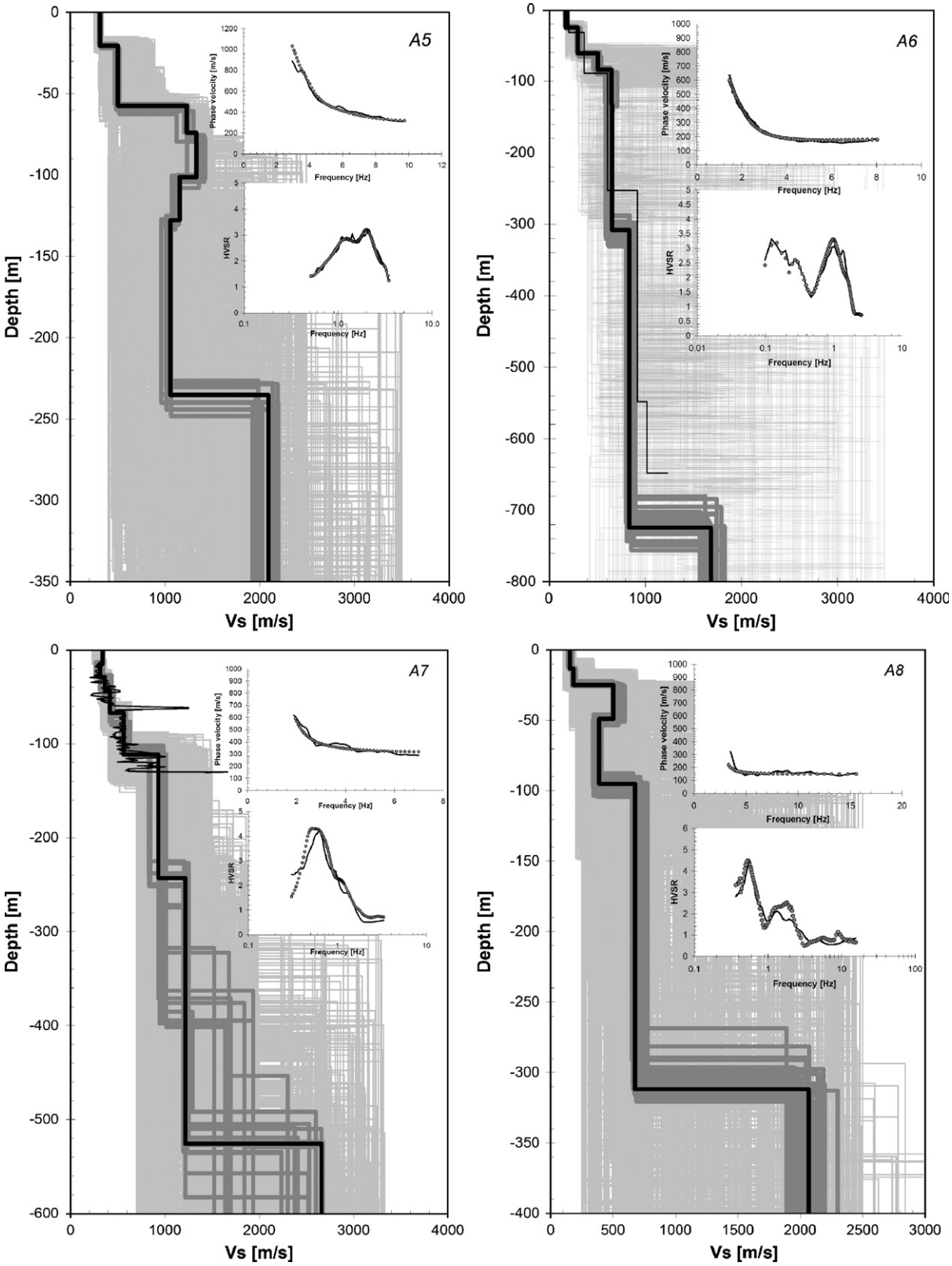

Fig. 9. Same as for Fig. 8, but for arrays A5, A6, A7 and A8. For array A6, the S-wave velocity profile from Kudo et al. [44] (thin black line) is also reported. For array A7, the S-wave velocity profile (thin black line) determined from Suspension PS Logging testing performed at Borehole SK-3 at the Ataköy Vertical Array Site (personal communication) is also reported.

shallower impedance contrasts could be responsible for the anomalous ground motion amplification observed [43] in the frequency range of interest for buildings (i.e., from about 0.5 to 10 Hz).

In the proximity of A6 in the Avcilar district, Kudo et al. [44] estimated the S-wave velocity profiles from circular array observations of microtremors using the SPAC method. It is worth noting in Fig. 9, the excellent agreement in the S-wave velocity

trend between the two estimates. Despite the H/V peak at the lower frequency being closer to the sensibility limit of our instrument, it allows velocity estimates for the deeper rock formation in good agreement with those obtained by the arrays A4, A5, A7 and A8, and a depth in agreement with A1.

Another fact that gives us confidence in our results is that the estimated S-wave velocity structure of A7, until a depth of about 120 m, is in good agreement with suspension PS Logging measurements performed at the Ataköy Vertical Array Site [50] (Fig. 9). Finally, arrays A2 and A3 also show a strong impedance contrast at a depth of about 100 m.

4.3. Theoretical site response

The final step in the 2D array recording analysis consists of estimating the theoretical site-response function, starting from the retrieved S-wave velocity profiles. The procedure followed is discussed in Parolai et al. [27], and is based on computing synthetic seismograms using the improved Thompson–Haskell propagator matrix method [33]. Synthetic seismograms are generated for a standard receiver configuration of 15 equally spaced receivers using a seismic source at 5 km depth, considering both the estimated sedimentary cover structures and a pure half-space model (i.e., the theoretical reference site). Then, all records were analyzed, and the results averaged. Finally, FFT spectra of recordings were calculated and the theoretical horizontal-to-vertical spectral ratios (*THV*) computed. Although this method provides a simplified wavefield with respect to reality (i.e., it does not take into account wave diffraction and scattering), it allows site-response functions to be obtained that are able to capture the main features of the experimental ones [27].

Fig. 10 shows the *THV* ratios at the surface station from synthetic seismograms considering the model obtained by the arrays, with the exception of A4, which is located on the Paleozoic bedrock. As expected for the presence of various high impedance contrasts in the S-wave velocity profile, both at large (>200 m) and medium (about 100 m) depths, high levels of amplification are observed for many models, both at low (around 0.5 Hz) and high (>1 Hz) frequencies. Despite the simplified synthetic wavefield, the presence of amplification higher than a factor of 2 over a wide frequency range for the *THV* ratio curves, provides a clear picture of the site-response complexity for the western part of Istanbul (Fig. 10).

Bakir et al. [51] identified the districts of Avcilar, Ataköy, Bakirköy and Fatih as areas of the city where heavier damage in the event of future earthquakes are expected due to resonance effects and quasi-coincidence with the eigenperiods of the typical

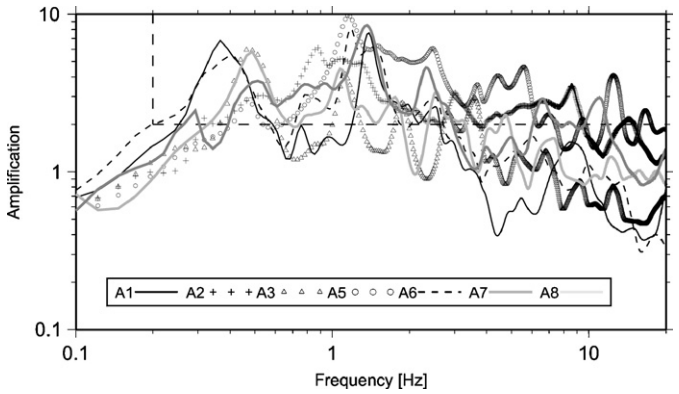

Fig. 10. H/V ratios at the surface station from synthetic seismograms considering the model obtained by the arrays. The dashed line bounds amplification higher than 2.

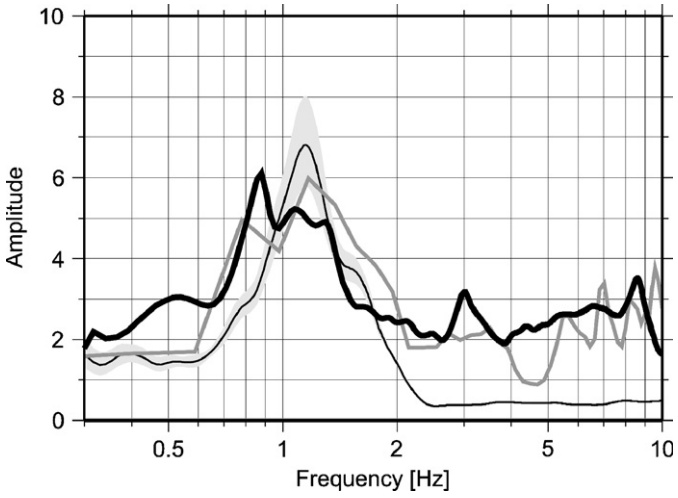

Fig. 11. IERRS station TOPKP. Average H/V spectral ratios from seismic noise (thin black line) ±95% confidence interval (grey area), H/V spectral ratios of an earthquake (dark grey line) with $M\sim4$ recorded by IERRS stations (Table 1), H/V ratios (thick black line) at the surface station from synthetic seismograms considering the model obtained by the array A2.

residential buildings in these areas. It is worth noting that for array A6 in Avcilar, high levels of amplification are estimated at both low (i.e., 0.5 Hz) and high frequencies (i.e., 1–2 Hz), in agreement with the observation of Bakir et al. [51] and [4,9] of a high site amplification hazard risk. Similar observations also hold for the Ataköy (A7) and Bakirköy (A8) districts, where the theoretical site response (Fig. 10) indicates, in agreement with theoretical studies [10] and experimental observations [34] ground motion amplifications well above a factor of 2 in the frequency range 0.2–10 Hz.

Finally, Fig. 11 shows the comparison between the *THV* ratio curves for the model of the array A2 located in the Fatih district, and the empirical *EHV* amplification function evaluated at the nearby (~1 km) IERRS station TOPKP (Fig. 1a). As shown by Harmandar et al. [41], the spatial variation of ground motion over this distance is very small, and the results can be reasonably compared. We note how the *THV* response is able to capture all of the main characteristics of the empirical *EHV*. In particular, differently from the H/V from seismic noise that only fits well the fundamental resonance peak (f_0) at about 1 Hz, the *THV* reproduces both f_0 and also the overall shape of the *EHV* in the frequency range from 2 to 10 Hz.

5. Conclusion

The western part of the megacity Istanbul has been studied by means of an extensive survey of environmental seismic noise measurements. Comparison of H/V curves from single station seismic noise measurements with those obtained by earthquake recordings indicates that the former are a good proxy for the fundamental resonance frequency. Therefore, a high number of single station seismic noise measurements has been carried out in western Istanbul allowing the mapping of fundamental resonance frequency. The fundamental frequency map is in remarkable agreement with the geological map, both in identifying the boundaries of the Paleozoic bedrock outcrops in the northern and eastern parts of the investigated area (characterized by H/V curves without amplification or fundamental resonance frequencies over 10 Hz), and the identification of areas with soft sedimentary covers in the southwestern part. Other studies [4,9,10,34,44,51] focused their activities only at sites characterized by the presence

of soft sediments. They concluded that such situations are responsible for the anomalous ground motion amplification during earthquakes. Our results confirm this conclusion, having, in addiction, a broader area coverage. In fact, the fundamental frequency map presented in this study provides a general overview of those area in the whole western Istanbul characterized by fundamental resonance frequencies that lie in the same range of those observed for the typical residential buildings in these regions (i.e., from 0.5 to 10 Hz).

Seismic noise measurements using 2D arrays were carried out in areas with different surficial geology. The joint inversion of Rayleigh wave dispersion and H/V curves, using a combination of different methods to manage the severe non-linearity of the problem, allowed the retrieval of the S-wave velocity structure for some hundreds of meters. The estimated S-wave velocity profiles confirm the existence of different mechanical structures in the western part of the metropolitan area, which are in most of the cases (A1, A2, A3, A5, A6, A7 and A8) characterized by strong impedance contrasts. The complex nature of such S-wave velocity structures determine theoretical site responses characterized, for most of the sites, by amplification factors well above than 2 in the frequency band from 0.2 to 10 Hz.

Comparing the theoretical site response from 2D arrays with the empirical ones from an earthquake recorded at the nearby seismic station TOPKP indicates that, 2D array seismic noise methods allow for the estimation of the most relevant and reliable information about the local S-wave structure for site response. Therefore, further 2D array seismic noise measurements and analysis will be subject of future investigations.

Acknowledgements

We are grateful to R. Milkereit, R. Bauz and E. Guenther for the fieldwork. Furthermore, we appreciated the help of the students from the Bogazici University. We thank M. Sørensen for useful discussions and Karin Sesetyan for the geological map of Istanbul. Moreover, we thank the people of the Municipality of Istanbul for the technical and human support. K. Fleming kindly improved the English. Some of the figures were generated using GMT [52] thanks to the help of R. Milkereit.

Appendix A. Supplementary materials

Supplementary data associated with this article can be found in the online version at doi:10.1016/j.soildyn.2008.05.007.

References

[1] Erdik M, Aydinoglu N, Fahjan Y, Sesetyan K, Demircioglu M, Siyahi B, et al. Earthquake risk assessment for Istanbul metropolitan area. Earthquake Eng Eng Vib 2003;2:1.
[2] Ambraseys NN, Finkel CF. Long-term seismicity of Istanbul and of the Marmara Sea region. Terra Nova 1991;3:527–39.
[3] Ozel O, Sasatani T, Kudo K, Okada H, Kanno T, Tsuno S, et al. Estimation of S-wave velocity structures in Avcilar–Istanbul from array microtremor measurements. Geophysics 2004;12:2.
[4] Tezcan SS, Kaya E, Bal LE, Özdemir Z. Seismic amplification at Avcilar, Istanbul. Eng Struct 2002;24:661–7.
[5] Beyen K, Erdik M. Two-dimensional nonlinear site response analysis of Adapazari plain and predictions inferred from aftershocks of the Kocaeli Earthquake of 17 August 1999. Soil Dyn Earthquake Eng 2004;24:261–79.
[6] Ansal A, Laue J, Buchheister J, Erdik M, Springman SM, Studer J, Koksal D. Site characterization and site amplification for a seismic microzonation study in Turkey. In: Proceedings of the 11th international conference on soil dynamics and earthquake engineering (11th ICSDEE) and the 3rd international conference on earthquake geotechnical engineering (3rd ICEGE), Berkeley, CA, 7–9 January 2004. p. 53–60.
[7] Gruenthal G. European macroseismic scale 1998. Cahiers du Centre Européen de Géodynamique et de Séismologie 1998;15:99.
[8] Ozmen B. Isoseismal Map of Izmit Earthquake. In: Izmit Körfezi Depreminin Hasar Durumu (Rakamsal Verilerle), damage in the İzmit Bay Earthquake (with quantitative data), Turkiye Deprem Vakli, Istanbul, 2004.
[9] Ergin M, Özalaybey S, Aktar M, Yalçin MN. Site amplification at Avcilar, Istanbul. Tectonophysics 2004;391:335–46.
[10] Sørensen M, Oprsal I, Bonnefoy-Claudet S, Atakan K, Martin Mai P, Pulido N, et al. Local site effects in Ataköy, Istanbul, Turkey, due to a future large earthquake in the Marmara Sea. Geophys J Int 2006;167:1413–24.
[11] Wald LA, Mori J. Evaluation of methods for estimating linear site-response amplifications in the Los Angeles Region. Bull Seism Soc Am 2000;90:S32–42.
[12] Stewart JP, Liu AH, Choi Y. Amplification factors for spectral acceleration in tectonically active regions. Bull Seism Soc Am 2003;93:332–52.
[13] Park D, Hashash YMA. Probabilistic seismic hazard analysis with non linear site effects in the Mississippi embayment In: Proceedings of the 13th world conference on earthquake engineering, Vancouver, CD-Rom edition 2004, paper no. 1549.
[14] Di Giacomo D, Gallipoli MR, Mucciarelli M, Parolai S, Richwalski SM. Analysis and modeling of HVSR in the presence of a velocity inversion: the case of Venosa, Italy. Bull Seism Soc Am 2005;95:2364–72.
[15] Mucciarelli, M., Gallipoli, MR., Comparison between Vs30 and other estimates of site amplification in Italy. In: First European conference on earthquake engineering and seismology (a joint event of the 13th ECEE and 30th General Assembly of the ESC), Geneva, Switzerland, 3–8 September 2006, paper no. 270.
[16] Fäh D, Kind F, Giardini D. A theoretical investigation of average H/V ratios. Geophys J Int 2001;145:535–49.
[17] Arai H, Tokimatsu K. S-wave velocity profiling by inversion of microtremor H/V spectrum. Bull Seism Soc Am 2004;94(1):53–63.
[18] Scherbaum F, Hinzen KG, Ohrnberger M. Determination of shallow shear wave velocity profiles in Cologne, Germany area using ambient vibrations. Geophys J Int 2003;152:597–612.
[19] Parolai S, Bormann P, Milkereit C. Assessment of the natural frequency of the sedimentary cover in the Cologne area (Germany) using noise measurements. J Earthquake Eng 2001;5(4):541–64.
[20] Parolai S, Bindi D, Baumbach M, Grosser H, Milkereit C, Karakisa S, et al. Comparison of different site estimation techniques using the Izmit 1999 earthquake aftershocks. Bull Seism Soc Am 2004;3:1096–108.
[21] Tokimatsu K, Tamura S, Kojima H. Effects of multiple modes on Rayleigh wave dispersion characteristics. J Geotech Eng 1992;118:1529–43.
[22] Ohori M, Nobata A, Wakamatsu K. A comparison of ESAC and FK methods of estimating phase velocity using arbitrarily shaped microtremor analysis Bull. Seism Soc Am 2002;92:2323–32.
[23] Parolai S, Richwalski SM, Milkereit C, Fäh D. S-wave velocity profiles for earthquake engineering purposes fort he Cologne area (Germany). Bull Earthquake Eng 2006;4:65–94.
[24] Parolai S, Picozzi M, Richwalski SM, Milkereit C. Joint inversion of phase velocity dispersion and H/V ratio curves from seismic noise recordings using a genetic algorithm, considering higher modes. Geophy Res Lett 2005;32: L01303.
[25] Arai H, Tokimatsu K. S-wave velocity profiling by joint inversion of microtremor dispersion curve and horizontal-to-vertical (H/V) spectrum. Bull Seism Soc Am 2005;95(5):1766–78.
[26] Picozzi M, Albarello D. Combining genetic and linearized algorithms for a two-step joint inversion of Rayleigh wave dispersion and H/V spectral ratio curves. Geophys J Int 2007;169:189.
[27] Parolai S, Mucciarelli M, Gallipoli MR, Richwalski SM, Strollo A. Comparison of empirical and numerical site responses at the Tito test site (Southern Italy). Bull Seism Soc Am 2007;97(5):1413–31.
[28] Richwalski SM, Picozzi M, Parolai S, Milkereit C, Baliva F, Albarello D, et al. Rayleigh wave dispersion curves from seismological and engineering-geotechnical methods: a comparison at the Bornheim test site (Germany). Bull Earthquake Eng 2007;4:349–61.
[29] Aki K. Space and time spectra of stationary stochastic waves, with special reference to microtremors. Bull Earthquake Res Inst 1957;35:415–56.
[30] Okada H. The Microtremor Survey Method (Geophysical Monograph Series 12). Washington: American Geophysical Union; 2003.
[31] Capon J. High-resolution frequency–wavenumber spectrum analysis. Proc IEEE 1969;57(8):1408–18.
[32] Horike M. Inversion of phase velocity of long period microtremors to the S-wave velocity structure down to the basement in urbanized areas. J Phys Earth 1985;33:59–96.
[33] Wang RA. Simple orthonormalization method for stable and efficient computation of Green's functions. Bull Seism Soc Am 1999;89:733–41.
[34] Birgören G, Özel O. Determination of site effects and ground motion lengthening in Istanbul area derived from small earthquake recordings. In: Proceedings of the 8th US national conference on earthquake engineering, San Francisco, CA, USA, 18–22 April 2006, paper no. 1908.
[35] Strollo A, Parolai S, Jäckell K-H, Marzorati S, Bindi D. The effect of seismic instrumentation using short-period electromagnetic sensors on seismic noise analysis in the frequency band 0.1–1 Hz. Bull Seism Soc Am 2007;98: 671–81.
[36] Strollo A, Bindi D, Parolai S, Jäckel K-H. On the suitability of 1 s geophone for ambient noise measurements in the 0.1–20 Hz frequency range: experimental outcomes. Bull Earthquake Eng, doi:10.1007/s10518-008-9061-x.

[37] Peterson J. Observations and modeling of seismic background noise. US Geol Surv Open-File Rep 1993;322:93–5.
[38] Picozzi M, Parolai S, Albarello D. Statistical analysis of noise horizontal to vertical spectral ratios (HVSR). Bull Seism Soc Am 2005;95.
[39] Nakamura Y. A method for dynamic characteristics estimation of subsurface using microtremor on the ground surface. Q Railway Tech Res Inst 1989;30:25–33.
[40] D'Amico V, Picozzi M, Albarello D, Naso G, Tropenscovino S. Quick estimate of soft sediments thickness from ambient noise horizontal-to-vertical spectral ratios: a case study in southern Italy. J Earthquake Eng 2004;8(6):895–908.
[41] Harmandar E, Durukal E, Erdik M, Ozel O. Spatial variation of ground motion in Istanbul. In: Poster presentation ID 1633, potential for very large earthquake disasters in the European Mediterranean region, European Geophysical Union, Vienna, 2006.
[42] Haghshenas E, Bard P-Y, Theodulidis N. SESAME WP04 Team. Empirical evaluation of microtremor H/V spectral ratio. Bull Earthquake Eng 2008;6: 75–108.
[43] Cranswick E, Ozel O, Meremonte M, Erdik M, Safak E, Mueller C, Overturf D, Frankel A. Earthquake damage, site response, and building response in Avcilar, West of Istanbul, Turkey. International Journal for Housing Science and Its Applications, ISSN 0146-6518, special issue: Kocaeli Earthquake 1999, Oktay Ural, editor-in-chief, vol. 24, no. 1, 2000. p. 85–96.
[44] Kudo K, Kanno T, Okada H, Ozel O, Erdik M, Sasatani T, et al. Site-specific issues for strong ground motions during the Kocaeli, Turkey, earthquake of 17 August 1999, as inferred from array observations of microtremors and aftershocks. Bull Seism Soc Am 2002;92(1):448–65.
[45] Wathelet M. Array recordings of ambient vibrations: surface-wave inversion. PhD thesis, Université de Liège, Faculté des Sciences Appliquées, 2005.
[46] Yamanaka H, Ishida H. Application of generic algorithms to an inversion of surface–wave dispersion data. Bull Seism Soc Am 1996;86:436–44.
[47] Herrmann RB. Computer programs in seismology, version 3.2, Saint Louis University, 2002.
[48] Herrmann RB, Ammon CJ, Julia J, Mokhtar T. Joint inversion of receiver functions and surface-wave dispersion for crustal structure. In: Proceedings of the 21st seismic research symposium technologies for monitoring the comprehensive nuclear test ban treaty, 21–24 September 1999, Las Vegas, NV, USA, Los Alamos National Laboratory, LA-UR-99-4700, 1999.
[49] Dalgiç S. Factor affecting the greater damage in the Avcilar area of Istanbul during the 17 August 1999 Izmit earthquake. Bull Eng Geol Environ 2004;63:221–32.
[50] Ansal AM, Kurtulus A. Suspension PS velocity logging measurements at Atakoy vertical array site, Istanbul, 2007 data report.
[51] Bakir PG, Roeck G, Degrande G, Reynders E. Seismic demands and analysis of site effects in the Marmara region during the 1999 Kocaeli Earthquake. Nat Hazards 2007;42(1):169–91.
[52] Wessel P, Smith WHF. Free software helps map and display data. EOS (AGU) 1991;72:445–6.